

Wearable Electrically Small Loop Antennas for Monitoring Joint Flexion and Rotation

Vigyanshu Mishra, *Student Member, IEEE*, and Asimina Kiourti, *Senior Member, IEEE*

Abstract—Wearable Electrically Small Loop Antennas (ESLAs) are introduced to monitor joint flexion and rotation while overcoming limitations in the state-of-the-art. The reported approach is not restricted to lab environments, does not suffer from integration drift and line-of-sight, and does not impede natural movement. Our previous work introduced wrap-around coils that addressed the challenges above, but were limited to monitoring joint flexion. By contrast, a new class of ESLAs is herewith proposed, placed longitudinally across the joint and operating at 34MHz to monitor both flexion and rotation. An added advantage vs. our previous design is a remarkable improvement in flexion angle resolution: the transmission coefficient dynamic range for 0° to 100° flexion improves by 18.8dB in this work. Two ESLAs are shown to accurately detect flexion/rotation for angular resolutions up to 10° . But if higher resolution is desired, ambiguities arise. To tackle this, a three-ESLA system with integrated post-processing is proposed that achieves resolution as high as 2° . Simulations and *in vitro* experiments are in excellent agreement. Guidelines for system design suited to diverse applications are discussed, and conformance with safety standards is ensured. In future, ESLAs can be seamlessly integrated in garments, enabling transformative benefits to healthcare, sports, and beyond.

Index Terms—Bioelectromagnetics, Electrically Small Loop Antenna (ESLA), joint flexion and rotation, wearables.

I. INTRODUCTION

HUMAN joints can flex and rotate, allowing for various complex movements. The vision of monitoring such movements in real-time, seamlessly, without obstructing natural movement, and in the individual's natural environment, may ultimately open doors for innumerable applications. Examples include monitoring of motor disabling conditions (caused due to Parkinson's, Traumatic Brain Injury (TBI), physical injury etc.) [1], [2], gesture recognition and human-machine interfaces for virtual reality applications [3], [4], monitoring of athletes' performance [5], collection of baseline data from healthy individuals, and better

Manuscript received May 7, 2019; revised July 30, 2019; accepted August 8, 2019. This work was supported by the National Science Foundation under Grant 1842531.

V. Mishra and A. Kiourti are with the ElectroScience Laboratory, Department of Electrical and Computer Engineering, The Ohio State University, Columbus, OH, 43212, USA (e-mails: mishra.186@osu.edu, kiourti.1@osu.edu).

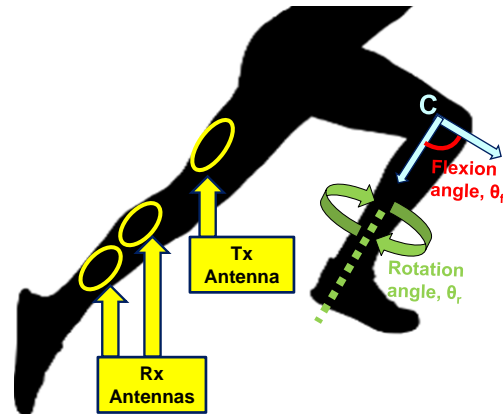


Fig. 1. Electrically Small Loop Antennas (ESLAs) used to monitor joint flexion and rotation.

understanding of obscure motor disabling diseases from a research perspective.

Currently, there are several technologies available to monitor joint motion. Despite having certain benefits, they suffer from inherent disadvantages which do not allow motion capture per the vision outlined above, Table I. Specifically, optical camera-based systems that rely on retro-reflective markers [6], [7] as well as their markerless versions [8], [9] are restricted to lab environments and line of sight. Antenna and other electromagnetics based techniques employ backscattering [10], radars [11], and Wi-Fi infrastructure [12] along with machine learning techniques to classify different activities (walking, sitting, jumping etc.). These are again restricted to closed/restricted environments and are focused on activity classification rather than precise motion monitoring (such as flexion, rotation, etc.). Inertial Measurement Units (IMUs) [13]-[15] break the lab boundaries but are unreliable (due to inherent drift) [13], [16] and not injury safe [17], [18]. Time-of-flight motion sensors that utilize ultra-wideband radios [19] or ultrasonic [16] systems to determine the time taken for a launched pulse to travel from transmitter to receiver are again restricted by line of sight and are obtrusive. Bending sensors that are worn directly on the joint to measure the produced strain (monitored as change in the sensor's resistance [20] or permeability [21]) obstruct natural movement and can withstand only limited number of cycles. Recently, we reported a new class of coils that wrap around the individual's limb to monitor joint flexion [22] while overcoming the challenges above. Unfortunately, these coils: (a) are restricted to only flexion monitoring, (b) are highly dependent on inter-/intra-subject variability of limb geometry

TABLE I
COMPARISON OF APPROACHES FOR MONITORING JOINT KINEMATICS

	Camera Based	Backscattering/ Radar/W-Fi Based	IMUs	Time-of-Flight	Bending Sensors	Wrap-Around Coils	Proposed
Works in unconfined environment	No (-)	No (-)	Yes (+)	Yes (+)	Yes (+)	Yes (+)	Yes (+)
Seamless	Yes (+)	Yes (+)	No (-)	No (-)	Yes (+)	Yes (+)	Yes (+)
Insensitive to Line-of-Sight	No (-)	No (-)	Yes (+)	No (-)	Yes (+)	Yes (+)	Yes (+)
Allows natural motion	Yes (+)	Yes (+)	Yes (+)	Yes (+)	No (-)	Yes (+)	Yes (+)
Reliable vs. time	Yes (+)	Yes (+)	No (-)	Yes (+)	No (-)	Yes (+)	Yes (+)
Monitors Joint Flexion	Yes (+)	No (-)	Yes (+)	Yes (+)	Yes (+)	Yes (+)	Yes (+)
Monitors Joint Rotation	Yes (+)	No (-)	Yes (+)	Yes (+)	Yes (+)	No (-)	Yes (+)
Independent of anatomical geometry of limb	Yes (+)	Yes (+)	Yes (+)	Yes (+)	Yes (+)	No (-)	Yes (+)
Flexion dynamic range (0° to 100°)	-	-	-	-	-	14.24 dB	33.03 dB (18.79 dB improvement)
Lower flexion angles that can be detected at ~0.1 dB sensitivity	-	-	-	-	-	10°	1.5° (6.7 times improvement)

(i.e., anatomical circumference), and (c) suffer from poor resolution, especially at lower flexion angles (for instance, change of merely 0.11 dB is observed when the flexion angle changes from 0° to 10°). In this work, we introduce a new class of Electrically Small Loop Antennas (ESLAs) that are placed longitudinally upon the limbs (i.e. plane of the ESLA is parallel to the axis of the limb, Fig. 1) to monitor motion while being robust to tissue variations and overcoming shortcomings in the state-of-the-art along with significantly outperforming our previously reported wrap-around coils [22], Table I.

In this paper, we begin with introducing the novel idea of employing ESLAs longitudinally across the joint to seamlessly monitor flexion and rotation. A two ESLA configuration is discussed first, illuminating the merit of the idea, yet indicating ambiguities under combined flexion and rotation scenarios for angular resolutions higher than 10°. To tackle this, a three-ESLA system with integrated post-processing is proposed, offering a resolution of 2° for combined flexion and rotation monitoring. Simulation results are presented and further validated by *in vitro* experiments. Guidelines for system design suited to diverse applications are discussed, followed by studies that explore conformance to electromagnetic safety standards for the Specific Absorption Rate (SAR).

II. OPERATING PRINCIPLE

As shown in Fig. 1, transmitter (Tx) and receiver (Rx) loop antennas are placed across the joint. Though focus of this work is on the knee joint, the approach is readily applicable to other joints as well. Flexion is achieved when the lower limb rotates with respect to the upper limb about the center 'C' of the joint, Fig. 2. At full extension, limbs are straight and the flexion angle is zero, $\theta_f = 0^\circ$. As the lower limb flexes about the joint, flexion angle (θ_f) increases. Similarly, the lower limb may also rotate (by angle θ_r) about the joint. In both flexion and rotation scenarios, the transmitter and receiver antennas get misaligned, leading to changes in the associated transmission coefficient(s). In turn, such changes can be monitored to identify the exact flexion or/and rotation angles.

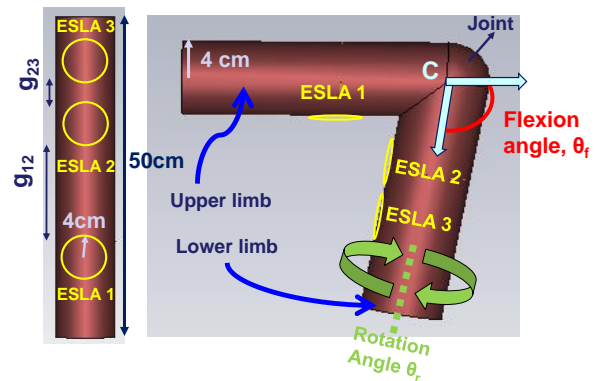


Fig. 2. Simulation set-up consisting of cylindrical limb and spherical joint made of 2/3 muscle. ESLA 1 is used as transmitter (Tx), while ESLA 2 and ESLA 3 are used as receivers (Rx).

In principle, the system of Fig. 2 can be realized using three modes of operation, viz. (a) electrically large loops (circumference $\sim \lambda$, where λ represents wavelength), (b) electrically small loops (circumference $< 0.1\lambda$) [23] or (c) in between both modes of operation ($0.1\lambda < \text{circumference} < \lambda$). Extensive frequency studies similar to those reported in [22] indicate that electrically small loops (ESLAs) operating at 34 MHz provide optimal performance in terms of: a) received power levels, b) resolution (smallest detectable angle), and c) robustness to changes in tissue properties.

The operating principle can be better understood using Faraday's law of induction [24]:

$$V_{Rx} = -\frac{d}{dt} \iint \mathbf{B}_{Tx} \cdot \widehat{\mathbf{n}}_{Rx} ds \quad (1)$$

where, \mathbf{B}_{Tx} is the transmitted magnetic flux density vector, $\widehat{\mathbf{n}}_{Rx}$ is the receiver area vector and V_{Rx} is the voltage induced on the receiver. Changes in flexion/rotation angle correspond to changes in the angle between $\widehat{\mathbf{n}}_{Rx}$ and \mathbf{B}_{Tx} . This gets reflected in V_{Rx} , and eventually captured in the transmission coefficient. That is, transmission coefficient becomes a function of flexion/rotation angle and hence can be used to monitor joint flexion and rotation.

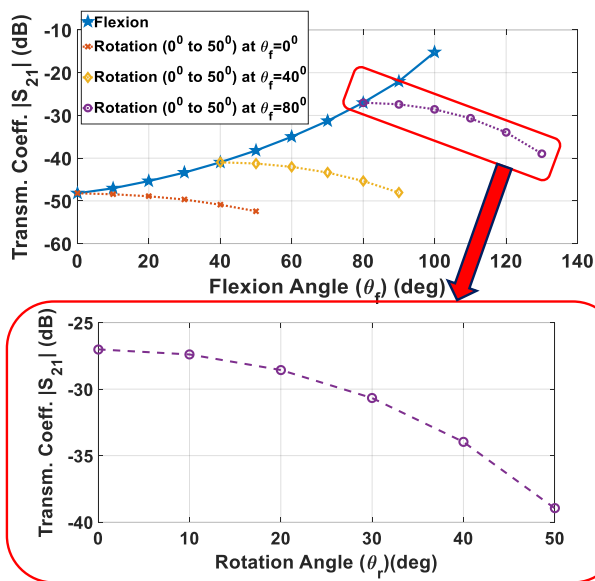


Fig. 3. Proof-of-concept results depicting changes in transmission coefficient ($|S_{21}|$) with varying flexion angle and rotation angle at 34 MHz. The bottom inset depicts an example rotation curve at $\theta_f = 80^\circ$.

As will be shown next, one transmitter and one receiver are enough to monitor joint flexion (at a given θ_r) or rotation (at a given θ_f). However, monitoring both flexion and rotation via a single transmitter/receiver pair leads to ambiguities for applications that require resolution higher than 10° . In other words, the same values of the transmission coefficient will end up corresponding to several different states of motion. To resolve ambiguities, two receiver antennas can be used. As such, Section III focuses on a two-ESLA configuration that will be used as a building block towards a three-ESLA configuration in Section IV.

III. TWO-ESLA CONFIGURATION

A. Simulations

The employed simulation set-up is shown in Fig. 2, where ESLA 1 serves as transmitter (Tx) and ESLA 2 as receiver (Rx). A homogenous (2/3 of muscle properties [25], [26]) cylindrical model is used as a first order approximation to human limbs, while the joint is modeled as a sphere. For this proof-of-concept model, the limb, joint and ESLA radius are set to 4 cm. Copper wire is used to realize the ESLAs (0.254 mm diameter), and a lumped capacitor (102 pF) is loaded on each of the ESLAs to introduce resonance and improve performance [22]. Gap between the ESLAs (g_{12}) in the extended state is set to 10 cm, in turn enabling flexion in the 0° to 100° range. Flexion ($\theta_f = 0^\circ$ to 100°) and rotation ($\theta_r = 0^\circ$ to 50°) are then incorporated in the model. For simulations, the frequency domain solver of CST Microwave Studio[®] (based on Finite Integral Technique) is used with tetrahedral meshing.

Simulated transmission coefficients ($|S_{21}|$) at the resonance frequency of 34 MHz are shown in Fig. 3. To provide a complete picture, Fig. 3 plots indicative rotation curves ($\theta_r = 0^\circ, 40^\circ$ and 80°) along with indicative flexion curves ($\theta_f = 0^\circ$

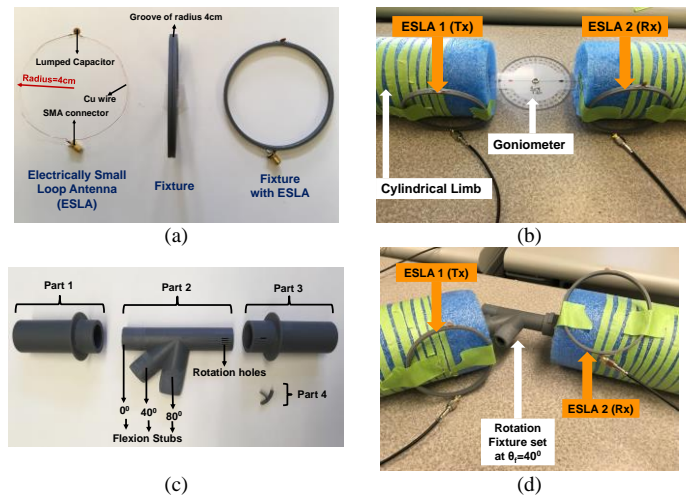


Fig. 4. (a) ESLA made of copper wire and subsequent integration in a 3D-printed fixture with a groove. (b) Flexion measurement set-up with goniometer, Styrofoam limbs and ESLAs connected to a network analyzer. (c) Fixture devised to enable controllable flexion and rotation (the four parts are eventually combined into one). (d) Combined flexion and rotation measurement set-up ($\theta_f = 40^\circ$ and $\theta_r = 50^\circ$).

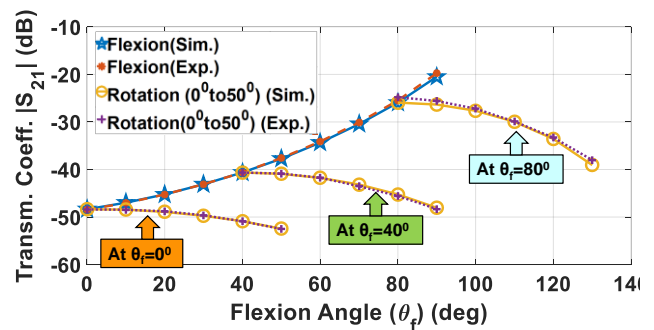


Fig. 5. Two-ESLA configuration: simulation and experimental results.

to 100° , at 10° steps). In this case, each rotation curve represents the change in $|S_{21}|$ as θ_r changes at a particular flexion angle. As an example, the rotation curve at $\theta_f = 80^\circ$ is shown in the inset of Fig. 3. As expected, changes in flexion and/or rotation angle imply significant changes in $|S_{21}|$. In other words, $|S_{21}|$ can be monitored to assess joint flexion and rotation.

B. Experimental Validation

ESLAs of radius 4 cm are fabricated using 30 AWG (0.254 mm diameter) copper wire and are further soldered to 102 pF lumped capacitors and SMA connectors, Fig. 4(a). To secure the coils, 3D-printed fixtures with a groove are used, Fig. 4(a). The limb is realized using cylindrical Styrofoam of radius 4 cm, as enabled by the insensitivity of ESLAs' performance in presence or absence of tissues (deduced from extensive frequency studies similar to [22]). A goniometer, commonly used to measure flexion angles in clinical practices, is inserted inside the upper/lower limbs, Fig. 4(b). The goniometer serves to emulate the flexing portion of the hinge joint while also assisting in setting up the intended flexion angle.

To incorporate controllable rotation into the design, the fixture of Fig. 4(c) is devised and 3D-printed. The fixture consists of four parts: parts 1 and 3 are fixed in the upper and

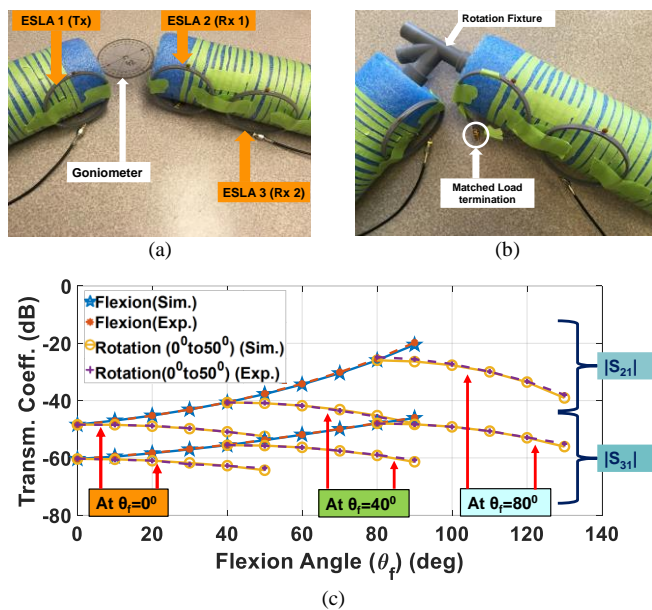


Fig. 6. Three-ESLA configuration: (a) measurement set-up for flexion monitoring using a goniometer, (b) measurement set-up for combined flexion and rotation monitoring using an in-house fixture, and (c) simulation and experimental results.

lower limbs, respectively; part 2 contains stubs for flexion at 0° , 40° , and 80° and holes for rotation from 0° to 50° at 10° steps; part 4 helps fix the desired rotation angle by aligning the rotation holes between part 2 and part 3. Fig. 4(d) depicts an example set-up with combined flexion and rotation ($\theta_f = 40^\circ$ and $\theta_r = 50^\circ$). To align with simulations, the fixture is designed such that the gap between the Tx and Rx ESLAs (g_{12}) is maintained at 10 cm for all flexion angles. For both flexion and rotation measurements, ESLAs are connected to the two ports of a PNA-L N5235A network analyzer.

Experimental results are shown in Fig. 5 and further superimposed with simulations. As seen, excellent agreement is achieved, further validating the ESLA approach for monitoring flexion and rotation angles.

C. Ambiguity Considerations

As is clearly indicated in Fig. 5, there is no one-to-one correlation between measured $|S_{21}|$ and associated flexion/rotation angles. For example, assuming a measurement of $|S_{21}| = -30$ dB, it is possible that ($\theta_f = 70^\circ$, $\theta_r = 0^\circ$) or ($\theta_f = 80^\circ$, $\theta_r = 30^\circ$), among others. Nevertheless, and as will become clear in Section IV.B, it is still possible to monitor both flexion and rotation using this configuration for applications that require resolution down to 10° . But for applications that require higher resolution, ambiguities arise in deciphering the right position of the limb. To tackle this, a three-ESLA configuration with integrated post-processing is discussed next. The results of Fig. 5 are, in turn, used as a building block toward the three-ESLA design.

IV. THREE-ESLA CONFIGURATION

A. Operating Principle

Using the three-ESLA configuration of Fig. 2, where ESLA 1 serves as transmitter (Tx) and ESLA 2 and ESLA 3 as

TABLE II
POST-PROCESSING FOR DIFFERENT ANGULAR RESOLUTIONS

Resolution	Total Data Points	Number of Ambiguities		Ambiguity Overlaps
		$ S_{21} $	$ S_{31} $	
10°	132	0	0	0
5°	462	1	1	0
3.3°	992	3	3	0
2.5°	1722	13	15	0
2°	2652	25	21	0
1.67°	3782	29	54	1
1.43°	5112	53	75	1
1.25°	6642	88	137	1
1.11°	8372	109	221	5
1°	10302	179	252	10

receivers (Rx), the same flexion and rotation angles are now captured by two different receivers. Notably, these receivers are positioned asymmetrically with respect to the transmitter, implying that asymmetric trends are anticipated in the $|S_{21}|$ and $|S_{31}|$ values. This is demonstrated in Section IV.B. In turn, ambiguous (θ_f , θ_r) pairs arising by the $|S_{21}|$ and $|S_{31}|$ curves will not be the same. Ideally, there should be only a single flexion/rotation angle combination that is identified by both $|S_{21}|$ and $|S_{31}|$ plots, and this will be the true and desired reading. This is discussed in Section IV.C.

B. Simulation and Experimental Results

Simulations are carried out using the three-ESLA configuration of Fig. 2. For this proof-of-concept design, ESLA 2 and ESLA 3 are separated by a gap (g_{23}) of 2 cm while ESLA 1 and ESLA 2 are separated by a gap (g_{12}) of 10 cm. Simulations are carried out for $\theta_f = 0^\circ$ to 100° (at steps of 10°) and $\theta_r = 0^\circ$ to 50° (at steps of 10° and at $\theta_f = 0^\circ$, 40° and 80°). Corresponding experiments are performed on the Styrofoam phantom of Fig. 4. For flexion-only monitoring, the employed set-up is shown in Fig. 6(a) where an inserted goniometer helps set the flexion angle. For combined flexion/rotation-monitoring, the 3D-printed fixture of Fig. 4 is employed, as shown in Fig. 6(b). Transmission coefficient values are measured using a two-port network analyzer, one receiver at a time. While taking $|S_{21}|$ measurements, ESLA 3 is terminated with a 50Ω load, and vice versa. This accounts for practical scenarios where both receivers are connected to 50Ω rather than being left open. Simulation and experimental results are depicted in Fig. 6(c) and are in excellent agreement.

C. Resolving Ambiguities

To evaluate the feasibility of resolving ambiguities, simulations are carried out for $\theta_f = 0^\circ$ to 100° (at 10° steps) and $\theta_r = 0^\circ$ to 50° (at 10° steps, and at $\theta_f = 0^\circ$ to 100° at 10° steps). The step size of 10° throughout these simulations sets the system resolution to 10° and leads to a total of 132 data points (i.e., $|S_{21}|$ and $|S_{31}|$ values). With precision set to two decimal digits, post-processing is performed in Matlab[®] to identify ambiguities in $|S_{21}|$ and $|S_{31}|$, and resolve them as needed. For a system resolution of 10° , no ambiguities are identified, implying that just a two-ESLA configuration is sufficient in this case. For a system resolution of lower than 10° , similar behavior is expected.

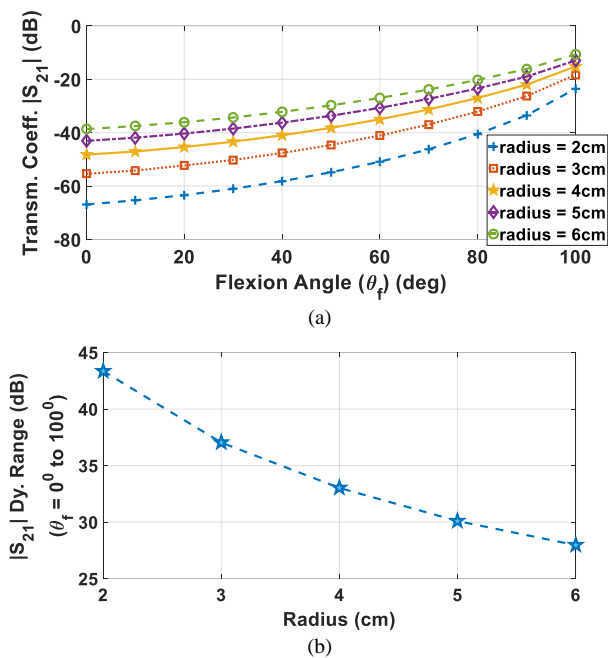


Fig. 9. (a) Flexion curves for different values of radius, and (b) increase of dynamic range ($|S_{21}|$) for flexion $\theta_f = 0^\circ$ to 100° with decrease in radius.

at $\theta_f < 30^\circ$. Nevertheless, fine-tuning of g_{12} , ESLA radius, and/or operation frequency may control/improve resolution, as outlined below.

1) Fine-tuning the ESLA gap

Considering g_{12} as the design parameter, and for flexion only scenario ($\theta_f = 0^\circ$), Fig. 7(a) plots flexion curves ($|S_{21}|$ vs θ_f) for different values of gaps (g_{12}). As seen, slope or dynamic range improves with decreasing g_{12} . To better visualize this, Fig. 7(b) plots the $|S_{21}|$ dynamic range (across $\theta_f = 0^\circ$ to 60° and $\theta_f = 0^\circ$ to 20°) as a function of g_{12} . Indeed, the dynamic range improves significantly with decrease in g_{12} even at smaller angles. Quantitative results are shown in Table III and are further compared vs. those of our previously reported wrap-around coils [22]. As seen, significant improvement is achieved.

For rotation, Fig. 8(a) (top) depicts the dynamic range variation vs. g_{12} at different θ_f , while Fig. 8(a) (bottom) depicts the dynamic range variation vs. θ_f at different g_{12} . At high θ_f , decrease in g_{12} helps improve the dynamic range (regardless of θ_f), however, it is not much useful at smaller θ_f . Also, it can be inferred that dynamic range for rotation is a function of both g_{12} and θ_f . Hence, Fig. 8(b) shows the intuitive effect of both parameters, depicting better dynamic range/resolution at higher θ_f and smaller g_{12} .

Following these guidelines, resolution of the three-ESLA configuration of Fig. 2 may increase to 0.4° for $g_{12} = 3$ cm as compared to 2° for $g_{12} = 10$ cm. Thus, using g_{12} as a design parameter, resolution of the complete system can be tweaked as required.

2) Fine-tuning the ESLA radius

Assuming a flexion only scenario ($\theta_f = 0^\circ$), Fig. 9(a) plots flexion curves for different ESLA radii, while Fig. 9(b) plots

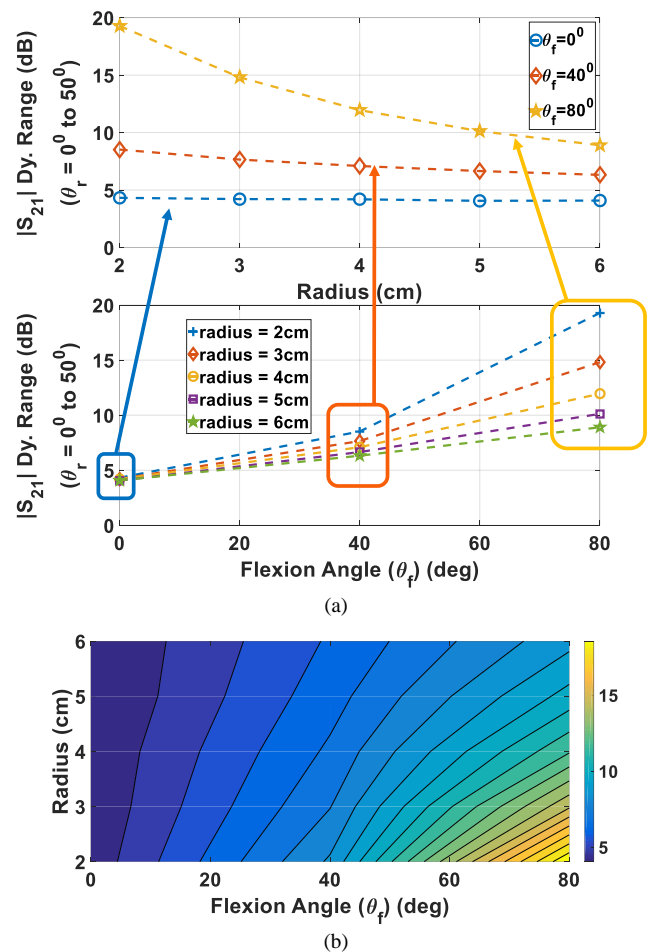


Fig. 10. Dynamic Range $|S_{21}|$ variation for rotation ($\theta_r = 0^\circ$ to 50°) (a) with θ_f for different values of radius and with radius for different values of θ_f , and, (b) contour plot depicting the variation with both radius and θ_f simultaneously. Better range is obtained for smaller radius and larger flexion angles.

the corresponding dynamic range. As seen, decrease in radius leads to better dynamic range for all θ_f values.

For rotation, radius variations depict very similar trends as those of g_{12} variations, Fig. 10. That is, better rotation resolution can be achieved at higher θ_f and at smaller radius values. The reason for this similar trend can be attributed to the fact that in both cases reduction in g_{12} or radius leads to more drastic changes in flux linkage with angular variation.

Similar to g_{12} , radius reduction will also help improve the resolution of the three-ESLA configuration of Fig. 2. Since the effect of both parameters is similar, analyses performed for g_{12} are not shown to avoid redundancy.

3) Fine-tuning the frequency

Considering frequency as a design parameter, similar to the discussion reported in [22], lower frequency of operation leads to better flexion resolution. This is also one of the reasons behind the selection of 34 MHz as the optimal operating frequency. However, frequency selection has relatively negligible effect on the rotation resolution.

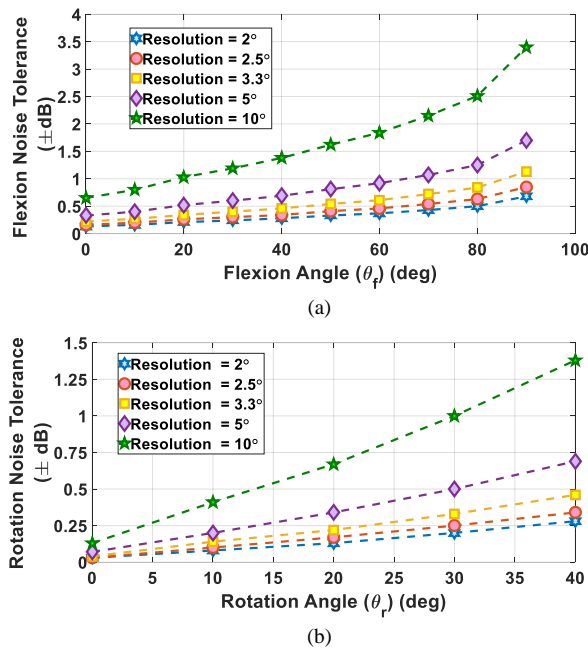


Fig. 11. Noise Tolerance (\pm dB) for (a) Flexion and (b) Rotation corresponding $|S_{21}|$, depicting decrease in chances of error as angle increases and resolution decreases.

B. Range of Motion and Power Reception

Range of motion (ROM) relates to the range of flexion (θ_f) and/or rotation (θ_r) angles. Ideally, higher range of motion is desirable. With the present configuration of two and three ESLAs, there is no limit on the rotation ROM irrespective of g_{12} , radius, or θ_f variation. However, decrease in g_{12} leads to reduction in flexion ROM as depicted in Fig. 7(a). This is because reduction in g_{12} results in transmit and receive ESLAs physically touching each other. Radius variation, on other hand, does not restrict flexion ROM, Fig. 9(a).

Power levels received by the Rx ESLA(s) are desired to be as high as possible. As is evident from Fig. 7(a) and 9(a), power reception improves with decrease in g_{12} and increase in radius, respectively. Similar trends are observed for the rotation curves as well.

In a nutshell, by decreasing g_{12} , power reception and resolution increase, but ROM decreases. By decreasing the ESLA radius, power reception reduces, resolution increases, and ROM remains unaffected. These imply a trade-off in the design, a conclusion which is equally valid for the three-ESLA system.

C. Insensitivity to tissue variation

System performance should be independent of tissue variations. An analysis similar to that performed in [22] has been repeated for the proposed ESLAs, indicating that frequencies in the inductive region are again suitable to meet this requirement. This is yet another reason for the choice of 34 MHz as the optimal operating frequency.

D. Specific Absorption Rate Studies

To ensure conformance with international safety guidelines, Specific Absorption Rate (SAR) studies are performed. The multi-layer arm model reported in [22] is employed, consisting

of 1.17 mm thick skin, 6.63 mm thick fat, 21.45 mm thick muscle, 4.68 mm thick cortical bone and 5.07 mm bone. For the two-ESLA and three-ESLA configuration, and assuming an input power of -15 dBm (as used in the experiments), maximum SAR averaged over 1g of tissue is equal to $1.44 \mu\text{W/Kg}$. This value is extremely low as compared to the safety limit of 1.6W/Kg set by Federal Communications Commission (FCC).

E. Error and Noise Considerations

Error and noise considerations become important, particularly when the system is intended to operate in dynamic or noisy environments. To this end, a noise tolerance analysis is hereafter performed that estimates the error handling capability of the system. Here, it is worth noting that the reported system is not designed for optimal noise tolerance capability. In other words, sensing of joint flexion/rotation via longitudinal ESLAs is not restricted to this analysis, and system design may readily be optimized in future for higher noise tolerance. However, our analysis does provide a baseline performance for noise tolerance.

Assuming operation in dynamic settings, the experimental data obtained can be compared vs. the calibration data to identify possible (θ_f, θ_r) values. In turn, noise tolerance can be determined from the calibration data themselves. In the following, simulation data is used as a calibration reference to perform this analysis. For a given system resolution and for a given data point ($|S_{21}|$) at a given θ_f or θ_r , half of the distance from that data point on either side will set the noise tolerance limit for that point. Now, if the noise in the experimental data exceeds this limit for that specific data point, the corresponding angle pair (θ_f, θ_r) obtained will be in error. In turn, this will lead to error in identifying the state of motion after post-processing. Reiterating this idea for all data points corresponding to each θ_f and θ_r , and for different resolutions, noise tolerance can be generated as shown in Fig. 11(a) and (b).

As expected, noise tolerance increases with increasing θ_f and θ_r (since $|\text{slope}|$ of $|S_{21}|$ vs. θ_f or θ_r increases with increasing θ_f or θ_r). Further, tolerance improves with decrease in system resolution, showing a tradeoff between the two. A similar analysis can be performed for $|S_{31}|$ data.

VI. CONCLUSION

In this work, a unique configuration of wearable ESLAs was introduced for seamlessly monitoring joint flexion and rotation. The reported approach (a) has the potential to break lab boundaries and enable monitoring in the individual's natural environment, (b) is not restricted by line-of-sight concerns (unlike optical cameras and time-of-flight sensors), (c) does not restrict natural motion (unlike bending sensors), (d) does not drift (unlike IMUs), and (e) can monitor both flexion and rotation (unlike wrap-around coils).

A two-ESLA configuration was reported first, able to monitor flexion and rotation at resolutions of 10° or lower. However, ambiguities were shown to arise for applications that require higher resolution. To tackle this, a three-ESLA configuration with accompanying post-processing was reported, achieving resolution of as high as 2° at an example

distance of 10 cm between the coils. Guidelines for system design suited to diverse applications in future, indicated that resolution may be further improved by fine-tuning the ESLA radius, ESLA separation, and ESLA operation frequency. Nevertheless, inherent trade-offs were identified in power reception and range of motion, which should be carefully accounted for during the design process.

The system may eventually be utilized for seamless motion capture in applications as diverse as healthcare, sports, virtual reality, human-machine interfaces and gesture recognition, among others. Future work will focus on (a) implementing the ESLAs on flexible e-textiles, (b) making the system wireless and portable, (c) validating *in vivo*, and (d) optimizing the system for higher noise tolerance in dynamic and real-world environments.

REFERENCES

- [1] Catarina Godinho, Josefa Domingos, Guilherme Cunha, Ana T. Santos, Ricardo M. Fernandes, Daisy Abreu, Nilza Gonçalves, Helen Matthews, Tom Isaacs, Joy Duffen, Ahmed Al-Jawad, Frank Larsen, Artur Serrano, Peter Weber, Andrea Thoms, Stefan Sollinger, Holm Graessner, Walter Maetzler and Joaquim J. Ferreira, "A systematic review of the characteristics and validity of monitoring technologies to assess Parkinson's disease," *Journal of NeuroEngineering and Rehabilitation*, vol. 13, no. 1, Mar 2016.
- [2] V. Bonnet, V. Joukov, D. Kulić, P. Fraisse, N. Ramdani and G. Venture, "Monitoring of hip and knee joint angles using a single inertial measurement unit during lower limb rehabilitation," *IEEE Sensors Journal*, vol. 16, no. 6, pp. 1557-1564, March, 2016.
- [3] T. P. Luu, Y. He, S. Brown, S. Nakagome, and J.L. Contreras-Vidal, "Gait adaptation to visual kinematic perturbations using a real-time closed-loop brain-computer interface to a virtual reality avatar," *Journal of Neural Engineering*, vol. 13, no. 3, Apr. 2016.
- [4] Y. Xiao, Z Zhang, A Beck, J Yuan, D. Thalmann, "Human-robot interaction by understanding upper body gestures," *Presence: Teleoperators and Virtual Environments*, vol. 23, no. 2, pp. 133-154, 2014.
- [5] H. Wagner, J. Pfusterschmied, M. Tilp, J. Landlinger, S.P. vonDuvillard, E.Muller, "Upper-body kinematics in team-handball throw, tennis serve, and volleyball spike," *Scandinavian Journal of Medicine and Science in Sports*, vol. 24, no. 2, pp. 345-354, Apr. 2014.
- [6] P. Eichelberger, M. Ferraro, U. Minder, T. Denton, A. Blasimann, F. Krause, H.Baur, "Analysis of accuracy in optical motion capture – A protocol for laboratory setup evaluation," *Journal of Biomechanics*, vol.49, Iss. 10, pp. 2085-2088, July 2016.
- [7] L. Herda, P. Fua, R. Plankers, R. Boulic, D. Thalmann, "Using skeleton-based tracking to increase the reliability of optical motion capture," *Human Movement Sciences*, vol. 20, Iss. 3, pp. 313-341, June 2001.
- [8] E. E. Stone and M. Skubic, "Unobtrusive, continuous, in-home gait measurement using the Microsoft Kinect," *IEEE Transactions on Biomedical Engineering*, vol. 60, no. 10, pp. 2925-2932, Oct. 2013.
- [9] F. Ferryanto and M. Nakashima, "Development of a markerless optical motion capture system for daily use of training in swimming," *Sports Engineering*, vol. 20, no. 1, pp. 63-72, Mar. 2017.
- [10] S. Amendola, L. Bianchi and G. Marrocco, "Movement detection of human body segments: passive radio-frequency identification and machine-learning technologies," *IEEE Antennas and Propagation Magazine*, vol. 57, no. 3, pp. 23-37, June 2015.
- [11] F. Qi, F. Liang, M. Liu, H. Lv, P. Wang, H. Xue, J. Wang, "Position-information-indexed classifier for improved through-wall detection and classification of human activities using UWB bio-radar," *IEEE Antennas and Wireless Propagation Letters*, vol. 18, no. 3, pp. 437-441, March 2019.
- [12] J. Liu, L Wang, J. Fang, L. Guo, B. Lu, L. Shu, "Multi-target intense human motion analysis and detection using channel state information," *Sensors*, 18, 3379, Oct. 2018.
- [13] M. El-Gohary and J. McNames, "Shoulder and elbow joint angle tracking with inertial sensors," *IEEE Transactions on Biomedical Engineering*, vol. 59, no. 9, pp. 2635-2641, Sept. 2012.
- [14] F.A. de Magalhaes, G. Vannozzi, G. Gatta and Silvia Fantozzi, "Wearable inertial sensors in swimming motion analysis: a systematic review," *Journal of Sports Sciences*, vol. 33, no. 7, pp. 732-745, 2015.
- [15] B. Mariani, M. C. Jiménez, F. J. G. Vingerhoets and K. Aminian, "On-shoe wearable sensors for gait and turning assessment of patients with Parkinson's disease," *IEEE Transactions on Biomedical Engineering*, vol. 60, no. 1, pp. 155-158, Jan. 2013.
- [16] C. Einsmann, M. Quirk, B. Muzal, B. Venkatramani, T. Martin and M. Jones, "Modeling a wearable full-body motion capture system," in Ninth IEEE International Symposium on Wearable Computers (ISWC'05), Osaka, 2005, pp. 144-151.
- [17] S.C. Mukhopadhyah, "Wearable sensors for human activity monitoring: a review," *IEEE Sensors Journal*, vol. 15, no. 3, pp. 1321-1330, Mar. 2015.
- [18] T. Shany, S. J. Redmond, M. R. Narayanan and N. H. Lovell, "Sensors-Based Wearable systems for monitoring of human movement and falls," in *IEEE Sensors Journal*, vol. 12, no. 3, pp. 658-670, March 2012.
- [19] Y. Qi, C. B. Soh, E. Gunawan, K. Low and A. Maskooki, "A novel approach to joint flexion/extension angles measurement based on wearable UWB radios," *IEEE Journal of Biomedical and Health Informatics*, vol. 18, no. 1, pp. 300-308, Jan. 2014.
- [20] J. H. M. Bergmann, S. Anastasova-Ivanova, I. Spulber, V. Gulati, P. Georgiou and A. McGregor, "An attachable clothing sensor system for measuring knee joint angles," *IEEE Sensors Journal*, vol. 13, no. 10, pp. 4090-4097, Oct. 2013.
- [21] G. Moreton, T. Meydan and P. Williams, "Investigation and characterization of a planar figure-of-eight coil as a curvature sensor," in 2017 IEEE SENSORS, Glasgow, 2017, pp. 1-3.
- [22] V. Mishra and A. Kiourti, "Wrap-around wearable coils for seamless monitoring of joint flexion," *IEEE Transactions on Biomedical Engineering*. doi: 10.1109/TBME.2019.2895293
- [23] C.A Balanis, "Loop Antennas" in *Antenna Theory Analysis and Design 4th ed.*, Wiley.
- [24] W.H. Hayt Jr., and J.A.Buck, "Time-Varying Fields and Maxwell's Equations" in *Engineering Electromagnetics 6th ed.*, Mc.Graw-Hill.
- [25] C. Furse, D. A. Christensen, C. H. Durney, "Electric and Magnetic Fields: Basic Concepts," in *Basic Introduction to Bioelectromagnetics 2nd ed.*, Boca Raton: CRC Press, 2009 pp. 30-34.
- [26] P. Soontornpipit et al., "Design of implantable microstrip antenna for communication with medical implants," *IEEE Transactions on Microwave Theory and Techniques*, vol. 52, no. 8, pp. 1944-1951, Aug. 2004.



Vidyanshu Mishra (S'18) earned Bachelor of Technology degree in electronics and communication engineering from PDPM Indian Institute of Information Technology, Design and Manufacturing, Jabalpur, Madhya Pradesh, India, in 2012, and Master of Technology degree in radio frequency design and technology from Indian Institute of Technology, Delhi, India, in 2015.

He is currently pursuing his PhD in Electrical and Electronics Engineering from The Ohio State University, ElectroScience Laboratory, Columbus OH, USA, under the supervision of Dr. Asimina Kiourti. In past, he has held research positions on different research projects at Center for Applied Research in Electronics, Indian Institute of Technology, Delhi, India and has served as Engineer in Wireless Planning and Coordination Wing, New Delhi and Wireless Monitoring Organization, Ahmedabad, Ministry of Communication and IT, Government of India. He has authored 4 journal papers and 6 conference papers till date. He has worked on various aspects of electromagnetics and his current research interests include electromagnetics for wearable and biomedical applications.

Mr. Mishra has received several awards and fellowships including the IEEE Microwave Theory and Techniques Society (MTT-S) Graduate Fellowship for Medical Applications for 2019, USNC-URSI 2019 Travel Fellowship, and University Fellowship for the year 2017-18 by The Ohio State University.



Asimina Kiourti (S'10, M'14, SM'19) received the Diploma degree in electrical and computer engineering from the University of Patras, Patras, Greece, in 2008, the M.Sc. degree in technologies for broadband communications from University College London, London, U.K., in 2009, and the Ph.D. degree in electrical and computer engineering from the National Technical University of Athens, Athens, Greece, in 2013.

She is currently an Assistant Professor of Electrical and Computer Engineering at The Ohio State University and the ElectroScience Laboratory, Columbus, OH, USA. From 2013 to 2016 she served as a Post-Doctoral Researcher and then a Senior Research Associate at the ElectroScience Laboratory. During her career, she has authored over 45 journal papers, 80 conference papers, 9 book chapters and 8 patents. Her research interests include bio-electromagnetics, wearable and implantable antennas, sensors for body area applications, and functionalized e-textiles..

Dr. Kiourti has received several awards and scholarships, including the URSI Young Scientist Award for 2018, the IEEE Engineering in Medicine and Biology Society (EMB-S) Young Investigator Award for 2014, the IEEE Microwave Theory and Techniques Society (MTT-S) Graduate Fellowship for Medical Applications for 2012, and the IEEE Antennas and Propagation Society (AP-S) Doctoral Research Award for 2011. She is currently serving as an Associate Editor for the IEEE Transactions on Antennas and Propagation, the IEEE Journal of Electromagnetics, RF and Microwaves in Medicine and Biology, and Advanced Electromagnetics.